2009 American Control Conference
Hyatt Regency Riverfront, St. Louis, MO, USA
June 10-12, 2009



# A Feedback based Load Shaping Strategy for Fuel Utilization Control in SOFC Systems

Tuhin Das and Ryan Weisman

*Abstract*— **Solid Oxide Fuel Cells are attractive energy conversion devices due to their fuel flexibility and high efficiency. Fuel utilization is a critical variable in SOFC systems that directly impacts efficiency and longevity. In this paper we propose a control strategy for mitigating drastic fluctuations in fuel utilization that arise during load transients. The strategy uses a feedback based dynamic input shaping approach. A preliminary control law derived from a model-based analysis forms the basis of this design. The strategy requires one fuel flow sensor upstream of the integrated fuel processor and admits convenient integration into a comprehensive hybrid fuel cell control algorithm.**

## I. NOMENCLATURE

| | |
|---|---|
| $C_v$ | Sp. heat at constant volume, *J/mol/K* |
| $F$ | Faraday's constant, $96485.34$ *Coul./mol* |
| $h$ | Enthalpy, *J* |
| $i$ | Current draw, *A* |
| $k$ | Anode recirculation fraction |
| $MW$ | Molecular weight, *kg/mol* |
| $\dot{M}_{in}$ | Anode inlet mass flow rate, *kg/s* |
| $\dot{M}_o$ | Anode exit mass flow rate, *kg/s* |
| $N$ | Number of moles, *moles* |
| $\dot{N}_f$ | Molar flow rate of fuel, *moles/s* |
| $\dot{N}_{in}$ | Anode inlet flow rate, *moles/s* |
| $\dot{N}_o$ | Anode exit flow rate, *moles/s* |
| $n$ | Number of electrons participating in electro-chemical reaction, $(= 2)$ |
| $P$ | Pressure, $Pa$ |
| $R_u$ | Universal Gas Constant, $8.314$ *J/mol/K* |
| $r_I$, $r_{II}$, $r_{III}$ | Rates of reforming reactions, *moles/s* |
| $r_e$ | Rate of electrochemical reaction, *moles/s* |
| $T$ | Temperature, *K* |
| $U$ | Utilization |
| $V$ | Volume, $m^3$ |
| $\mathcal{N}_{cell}$ | Number of cells |
| $\dot{\eta}$ | Molar flow rate, *moles/s* |
| $\mathcal{R}$ | Species rate of formation, *moles/s* |
| $\mathcal{X}$ | Species mole fraction |
| $a$ | Anode control volume |
| $ex$ | Exit condition of control volume |
| $g$ | Gas control volume |
| $in$ | Inlet condition of control volume |
| $j$ | Values of 1 - 7 represent species $CH_4$, $CO$, $CO_2$, $H_2$, $H_2O$, $N_2$, and $O_2$ |
| $r$ | Reformate control volume |
| $ss$ | Steady-state |

This work was supported in part by Office of Naval Research under the grant #N000140810704. Tuhin Das is an assistant professor and Ryan Weisman is a graduate student of Mechanical Engineering, Rochester Inst. of Tech., 76 Lomb Memorial Drive, Rochester, NY 14623, tkdeme@rit.edu

## II. INTRODUCTION

Among different fuel cell technologies, Solid Oxide Fuel Cell (SOFC) systems have generated considerable interest in recent years. Fuel flexibility and tolerance to impurities are attractive attributes of SOFC systems. Their high operating temperatures ($800$°C to $1000$°C) are conducive to internal reforming of fuel. The exhaust gases are excellent means for sustaining on-board fuel reforming processes. SOFC systems are not only tolerant to carbon monoxide but can also use it as a fuel. They also serve as excellent combined heat and power (CHP) systems.

SOFC systems have typically been considered more for stationary applications. However, recently there is a thrust to use SOFCs in portable units or as Auxilliary Power Units (APU's) in mobile applications. While for stationary power applications performance requirements may be moderate in terms of load-following capability, it is not so for portable/mobile applications. In the later case, power fluctuations are significant and frequent, and superior load-following capability is desired without compromising stack life. SOFCs have limited dynamic load following capability that must be enhanced to make SOFC a competetive technology, [11].

An important performance variable of SOFCs is fuel utilization $U$. Utilization is the ratio (often expressed in percentage) of hydrogen consumption to the net available hydrogen in the anode. While high utilization implies high efficiency, very high utilization leads to reduced partial pressure of hydrogen in the fuel cell anode, which can cause irreversible damages due to anode oxidation [12]. Typically, $80 - 90\%$ is the target range of fuel utilization for achieving high efficiency over a wide range of operating conditions. In applications with significant power transients, the resulting fluctuations in the fuel utilization and repeated and prolonged deviation from target can adversely affect stack life.

In this paper, we address the aforementioned issue through the development of a feedback control strategy that significantly reduces the transients in utilization in the presence of transient power demand. The strategy comprises of a feedback based input shaping algorithm used in conjunction with analytical closed-form relationships derived from a non-linear state-space model of the system. The resulting regulation of the fuel cell current results in a deficit or surplus of power delivered by the fuel cell. This mismatch is resolved by hybridizing the fuel cell with a supplementary power source such as a battery or super-capacitor. The proposed fuel utilization control strategy fits directly with an overall power splitting control for the complete hybrid fuel cell system.

978-1-4244-4524-0/09/$25.00 ©2009 AACC

While earlier research has addressed the control of such systems, a majority has considered the Polymer Electrolyte Membrane (PEM) fuel cell technology. Control algorithms for hybrid PEMFC systems have been proposed in [2], [5], [9], [14], [15] and [16]. However, the health monitoring aspects of PEMFC systems are not emphasized in these papers. In [17], the authors address constraint handling in PEMFC systems. In comparison to PEMFC, few works on power management and control of hybrid SOFC systems appear in the literature, [7]. This is attributed to the earlier state of development of the SOFC technology and also to the increased complexity of sensing and estimation in SOFCs. Due to its fuel flexibility, an SOFC is typically supplied with a gas mixture consisting of several species, in comparison to pure hydrogen in case of PEMFC. Hence an accurate measurement of fuel utilization in SOFCs would require a number of species specific concentration sensors. Such sensors are avoided due to cost and reliability considerations. Our proposed control law only uses measurement of fuel flowrate at the fuel reformer inlet to achieve a significant reduction in transient utilization, while not requiring prior knowledge of the dynamic behavior of the fuel supply system.

We have adopted a model based approach where a detailed control-oriented mathematical model of an SOFC system is developed. The model captures the thermodynamics, chemical kinetics, heat transfer and pressure dynamics phenomena of the fuel cell in detail. The model has been validated against published results in [10], [12]. A system description and an overview of the system model are first presented. From an analytical treatment of the model, a set of steady-state relations are derived, detailed in one of our earlier papers [4]. Using the steady-state results as a preliminary control law, we demonstrate the effect of load transients on fuel utilization. The proposed feedback control strategy is presented next. A variety of simulation results are shown to illustrate the effectiveness of the control strategy. We then incorporate the proposed control strategy within a overall power-split control for a hybrid fuel cell system and present simulation results. Finally we state the concluding remarks.

## III. SYSTEM OVERVIEW

Our analysis is based on a steam reformer based tubular SOFC system. The system consists of three primary components, namely, the steam reformer which produces a hydrogen-rich gas from a mixture of methane and steam, the solid oxide fuel cell which generates electricty from electrochemical reactions, and the combustor where excess fuel is burnt to generate heat. Methane is chosen as the fuel for the system, with a molar flow rate of $\dot{N}_f$. It is noted here that the analysis and control development approach can be extended to other fuels as well, such as methanol, ethanol, etc. The SOFC system is described in Fig.1.

The reformer produces a hydrogen-rich gas which is supplied to the anode of the fuel cell. Electrochemical reactions occuring at the anode due to current draw results in a steam-rich gas mixture at the anode exit. A fraction $k$ of the anode

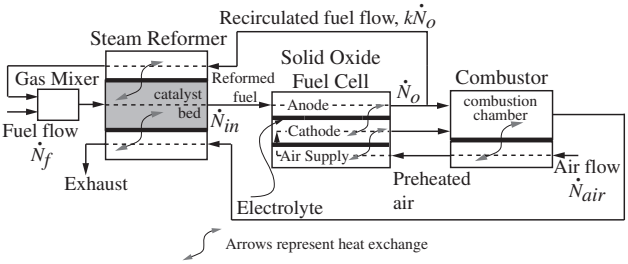


Fig. 1. Schematic diagram of the SOFC system

efflux is recirculated through the reformer into a mixing chamber where fuel is added. The recirculation $k$ is assumed to a fixed known fraction. In tubular SOFCs, recirculation is typically achieved through the deliberate use of imperfect seals. The mixing of the two fluid streams and pressurization is achieved in the gas mixer using an ejector or a recirculating fuel pump, [6]. The steam reforming process occuring in the reformer catalyst bed is an endothermic process. The energy required to sustain the process is supplied from two sources, namely, the combustor efflux that is passed through the reformer, and the aforementioned recirculated anode flow, as shown in Fig.1. The remaining anode efflux is mixed with the cathode efflux in the combustion chamber. The combustor also serves to preheat the cathode air which has a molar flow rate of $\dot{N}_{air}$. The tubular construction of each cell causes the air to first enter the cell through the air supply tube and then reverse its direction to enter the cathode chamber. The cathode air serves as the source of oxygen for the fuel cell.

## IV. SYSTEM MODEL

The essential dynamics of the SOFC system in Fig.1 are modeled using fundamental solid volume and gas control volume models. An overview of the mass and energy balance is provided below. The mass balance equation for individual species is constructed as follows,

$$\dot{N}_g \mathcal{X}_{j,g} + N_g \dot{\mathcal{X}}_{j,g} = \dot{\eta}_{in} \mathcal{X}_{j,in} - \dot{\eta}_{ex} \mathcal{X}_{j,g} + \mathcal{R}_{j,g}, \quad (1)$$

where specific values of subscripts $j$, $j = 1, 2, \cdots, 7$, correspond to the species $CH_4$, $CO$, $CO_2$, $H_2$, $H_2O$, $N_2$, and $O_2$ respectively. From Eq.(1), we additionally have

$$\begin{array}{c} \sum_{j=1}^{7} \mathcal{X}_{j,in} = \sum_{j=1}^{7} \mathcal{X}_{j,g} = 1 \;\Rightarrow\; \sum_{j=1}^{7} \dot{\mathcal{X}}_{j,g} = 0 \\ \Rightarrow\; \dot{N}_g = \dot{\eta}_{in} - \dot{\eta}_{ex} + \sum_{j=1}^{7} \mathcal{R}_{j,g} \end{array} \quad (2)$$

Flow rates are assumed to be governed by the pressure dynamics according to the following Darcian effect

$$\Delta P = MW_g \, \dot{\eta}_{ex} / k_d \quad (3)$$

where, $\Delta P$ is the pressure drop across adjacent control volumes and $k_d$ is a constant based on fluid properties and geometry. The temperature variations in a control volume is computed using the following energy balance equation

$$C_{v,g} \left( \dot{N}_g T_g + N_g \dot{T}_g \right) = \dot{h}_{in} - \dot{h}_{ex} + \dot{h}_{react} + \dot{Q} \quad (4)$$

The instantaneous pressure in a control volume is computed using the ideal gas law, $P_g V_g = N_g R_u T_g$.

### A. Reformer Model

For steam reforming of methane we consider a packed-bed tubular reformer with nickel-alumina catalyst [8], as shown in Fig.2. The exhaust, reformate and recirculated flows are

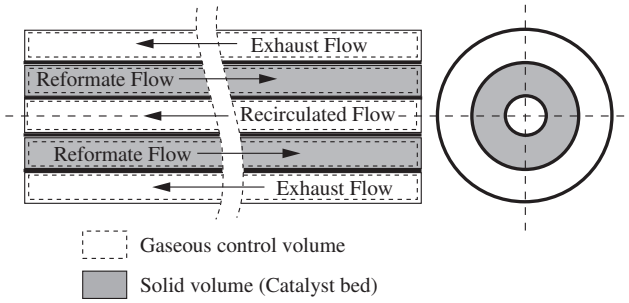


Fig. 2. Schematic diagram of tubular steam reformer

modeled using gas control volumes and the catalyst bed is modeled as a solid volume. The three main reactions in steam reforming of methane are, [18]:

$$\begin{array}{lrcl} \text{(I)} & CH_4 + H_2O & \leftrightarrow & CO + 3H_2 \\ \text{(II)} & CO + H_2O & \leftrightarrow & CO_2 + H_2 \\ \text{(III)} & CH_4 + 2H_2O & \leftrightarrow & CO_2 + 4H_2 \end{array} \tag{5}$$

From Fig.1, the mass balance equations for $CH_4$, $CO$, $CO_2$, $H_2$ and $H_2O$ can be written using Eq.(1) as follows:

$$\begin{aligned} \dot{N}_r\mathcal{X}_{1,r} + N_r\dot{\mathcal{X}}_{1,r} &= k\dot{N}_o\mathcal{X}_{1,a} - \dot{N}_{in}\mathcal{X}_{1,r} + \mathcal{R}_{1,r} + \dot{N}_f \\ \dot{N}_r\mathcal{X}_{2,r} + N_r\dot{\mathcal{X}}_{2,r} &= k\dot{N}_o\mathcal{X}_{2,a} - \dot{N}_{in}\mathcal{X}_{2,r} + \mathcal{R}_{2,r} \\ \dot{N}_r\mathcal{X}_{3,r} + N_r\dot{\mathcal{X}}_{3,r} &= k\dot{N}_o\mathcal{X}_{3,a} - \dot{N}_{in}\mathcal{X}_{3,r} + \mathcal{R}_{3,r} \\ \dot{N}_r\mathcal{X}_{4,r} + N_r\dot{\mathcal{X}}_{4,r} &= k\dot{N}_o\mathcal{X}_{4,a} - \dot{N}_{in}\mathcal{X}_{4,r} + \mathcal{R}_{4,r} \\ \dot{N}_r\mathcal{X}_{5,r} + N_r\dot{\mathcal{X}}_{5,r} &= k\dot{N}_o\mathcal{X}_{5,a} - \dot{N}_{in}\mathcal{X}_{5,r} + \mathcal{R}_{5,r} \end{aligned} \tag{6}$$

where $N_r = P_rV_r/R_uT_r$. From Eq.(5), we express $\mathcal{R}_{j,r}$, $j = 1, 2, \cdots, 5$, in terms of the reaction rates $r_I$, $r_{II}$ and $r_{III}$ as follows

$$\mathbf{R}_r = \mathbf{G}\,\mathbf{r},\ \mathbf{G} = \begin{bmatrix} -1 & 0 & -1 \\ 1 & -1 & 0 \\ 0 & 1 & 1 \\ 3 & 1 & 4 \\ -1 & -1 & -2 \end{bmatrix},\ \mathbf{R}_r = \begin{bmatrix} \mathcal{R}_{1,r} \\ \mathcal{R}_{2,r} \\ \mathcal{R}_{3,r} \\ \mathcal{R}_{4,r} \\ \mathcal{R}_{5,r} \end{bmatrix} \tag{7}$$

$\mathbf{r} = [r_I, r_{II}, r_{III}]^T$. Since $\mathbf{G}$ has a rank of 2, therefore there are only two independent reaction rates among $\mathcal{R}_{j,r}$, $j = 1, 2, \cdots, 5$. Considering the rate of formation of $CH_4$ and $CO$ in the reformer to be independent, we can rewrite Eq.(6) as follows:

$$\begin{aligned} \dot{N}_r\mathcal{X}_{1,r} + N_r\dot{\mathcal{X}}_{1,r} &= k\dot{N}_o\mathcal{X}_{1,a} - \dot{N}_{in}\mathcal{X}_{1,r} + \mathcal{R}_{1,r} + \dot{N}_f \\ \dot{N}_r\mathcal{X}_{2,r} + N_r\dot{\mathcal{X}}_{2,r} &= k\dot{N}_o\mathcal{X}_{2,a} - \dot{N}_{in}\mathcal{X}_{2,r} + \mathcal{R}_{2,r} \\ \dot{N}_r\mathcal{X}_{3,r} + N_r\dot{\mathcal{X}}_{3,r} &= k\dot{N}_o\mathcal{X}_{3,a} - \dot{N}_{in}\mathcal{X}_{3,r} - \mathcal{R}_{1,r} - \mathcal{R}_{2,r} \\ \dot{N}_r\mathcal{X}_{4,r} + N_r\dot{\mathcal{X}}_{4,r} &= k\dot{N}_o\mathcal{X}_{4,a} - \dot{N}_{in}\mathcal{X}_{4,r} - 4\mathcal{R}_{1,r} - \mathcal{R}_{2,r} \\ \dot{N}_r\mathcal{X}_{5,r} + N_r\dot{\mathcal{X}}_{5,r} &= k\dot{N}_o\mathcal{X}_{5,a} - \dot{N}_{in}\mathcal{X}_{5,r} + 2\mathcal{R}_{1,r} + \mathcal{R}_{2,r} \end{aligned} \tag{8}$$

From Eqs.(2) and (8) we deduce

$$\dot{N}_r = k\dot{N}_o - \dot{N}_{in} + \dot{N}_f - 2\mathcal{R}_{1,r} \tag{9}$$

### B. SOFC Model

We assume our system to be comprised of $\mathcal{N}_{cell}$ tubular Solid Oxide Fuel Cells, connected in series. A schematic diagram of an individual cell is shown in Fig.3. The anode,

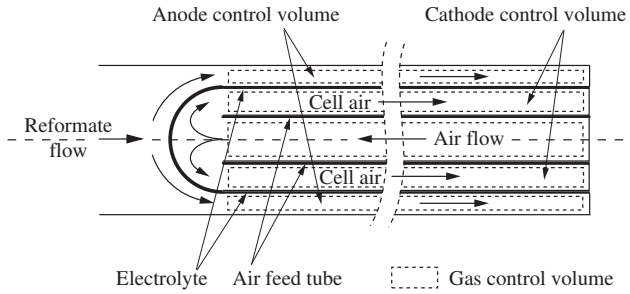


Fig. 3. Schematic diagram of tubular SOFC

cathode and air flows are modeled using gas control volumes. The air feed tube and the electrolyte are modeled as solid volumes. The following chemical and electro-chemical reactions occur simultaneously in the anode control volume:

$$\begin{array}{lrcl} \text{(I)} & CH_4 + H_2O & \leftrightarrow & CO + 3H_2 \\ \text{(II)} & CO + H_2O & \leftrightarrow & CO_2 + H_2 \\ \text{(III)} & CH_4 + 2H_2O & \leftrightarrow & CO_2 + 4H_2 \\ \text{(IV)} & H_2 + O^{2-} & \rightarrow & H_2O + 2e \end{array} \tag{10}$$

Steam reforming, represented by reactions I, II and III, occur in the anode due to high temperatures and the presence of nickel catalyst. The primary electrochemical process is steam generation from $H_2$, described by reaction IV. Simultaneous electrochemical conversion of $CO$ to $CO_2$ in the anode is also possible. However, this electro-chemical reaction is ignored since its reaction rate is much slower in presence of reactions II and IV, as indicated in [3] and references therein.

From Fig.1 and Eq.(1), the mass balance equations for $CH_4$, $CO$, $CO_2$, $H_2$ and $H_2O$ can be written as

$$\begin{aligned} \dot{N}_a\mathcal{X}_{1,a} + N_a\dot{\mathcal{X}}_{1,a} &= -\dot{N}_o\mathcal{X}_{1,a} + \dot{N}_{in}\mathcal{X}_{1,r} + \mathcal{R}_{1,a} \\ \dot{N}_a\mathcal{X}_{2,a} + N_a\dot{\mathcal{X}}_{2,a} &= -\dot{N}_o\mathcal{X}_{2,a} + \dot{N}_{in}\mathcal{X}_{2,r} + \mathcal{R}_{2,a} \\ \dot{N}_a\mathcal{X}_{3,a} + N_a\dot{\mathcal{X}}_{3,a} &= -\dot{N}_o\mathcal{X}_{3,a} + \dot{N}_{in}\mathcal{X}_{3,r} + \mathcal{R}_{3,a} \\ \dot{N}_a\mathcal{X}_{4,a} + N_a\dot{\mathcal{X}}_{4,a} &= -\dot{N}_o\mathcal{X}_{4,a} + \dot{N}_{in}\mathcal{X}_{4,r} + \mathcal{R}_{4,a} - r_e \\ \dot{N}_a\mathcal{X}_{5,a} + N_a\dot{\mathcal{X}}_{5,a} &= -\dot{N}_o\mathcal{X}_{5,a} + \dot{N}_{in}\mathcal{X}_{5,r} + \mathcal{R}_{5,a} + r_e \end{aligned} \tag{11}$$

where $N_a = P_aV_a/R_uT_a$ and $r_e$ is the rate of electrochemical reaction given by

$$r_e = i\mathcal{N}_{cell}/nF \tag{12}$$

Since current $i$ can be measured, the rate of electrochemical reaction $r_e$ is considered known. As with the reformate control volume, the anode inlet and exit flows do not contain $O_2$ and $N_2$. Therefore, $\mathcal{X}_{6,a} = \mathcal{X}_{7,a} = 0$. From Eq.(10), we express $\mathcal{R}_{j,a}$, $j = 1, 2, \cdots, 5$, in terms of the reaction rates $r_I$, $r_{II}$ and $r_{III}$ as follows

$$\mathbf{R}_a = \mathbf{G}\,\mathbf{r} + r_e\,[0\ \ 0\ \ 0\ \ -1\ \ 1]^T \tag{13}$$

where $\mathbf{R}_a = [\mathcal{R}_{1,a}\ \mathcal{R}_{2,a}\ \mathcal{R}_{3,a}\ \mathcal{R}_{4,a}\ \mathcal{R}_{5,a}]^T$, and $\mathbf{G}$ and $\mathbf{r}$ are given in Eq.(7). Since $\mathbf{G}$ has a rank of 2 and $r_e$ is

known, therefore there are only two independent reaction rates among $\mathcal{R}_{j,a},\ j = 1, 2, \cdots, 5$. Considering $\mathcal{R}_{1,a}$ and $\mathcal{R}_{2,a}$ to be independent, we can rewrite Eq.(11) as

$$\begin{aligned}
\dot{N}_a\mathcal{X}_{1,a}+N_a\dot{\mathcal{X}}_{1,a} &= \dot{N}_{in}\mathcal{X}_{1,r}-\dot{N}_o\mathcal{X}_{1,a}+\mathcal{R}_{1,a}\\
\dot{N}_a\mathcal{X}_{2,a}+N_a\dot{\mathcal{X}}_{2,a} &= \dot{N}_{in}\mathcal{X}_{2,r}-\dot{N}_o\mathcal{X}_{2,a}+\mathcal{R}_{2,a}\\
\dot{N}_a\mathcal{X}_{3,a}+N_a\dot{\mathcal{X}}_{3,a} &= \dot{N}_{in}\mathcal{X}_{3,r}-\dot{N}_o\mathcal{X}_{3,a}-\mathcal{R}_{1,a}-\mathcal{R}_{2,a}\\
\dot{N}_a\mathcal{X}_{4,a}+N_a\dot{\mathcal{X}}_{4,a} &= \dot{N}_{in}\mathcal{X}_{4,r}-\dot{N}_o\mathcal{X}_{4,a}-4\mathcal{R}_{1,a}-\mathcal{R}_{2,a}-r_e\\
\dot{N}_a\mathcal{X}_{5,a}+N_a\dot{\mathcal{X}}_{5,a} &= \dot{N}_{in}\mathcal{X}_{5,r}-\dot{N}_o\mathcal{X}_{5,a}+2\mathcal{R}_{1,a}+\mathcal{R}_{2,a}+r_e
\end{aligned} \tag{14}$$

From Eqs.(2) and (14) we deduce that

$$\dot{N}_a = \dot{N}_{in} - \dot{N}_o - 2\mathcal{R}_{1,a} \tag{15}$$

The cathode control volume and the cell voltage models are not of direct relevance to the development of the proposed control strategy and hence are omitted.

## V. STEADY-STATE RESULTS

Based on the state variable definitions in Eqs.(8) and (14), fuel utilization can be expressed as follows:

$$U = 1 - \frac{\dot{N}_o\left(4\mathcal{X}_{1,a}+\mathcal{X}_{2,a}+\mathcal{X}_{4,a}\right)}{\dot{N}_{in}\left(4\mathcal{X}_{1,r}+\mathcal{X}_{2,r}+\mathcal{X}_{4,r}\right)} \tag{16}$$

Eq.(16) is based on the internal reforming capability of the anode where a $CH_4$ and a $CO$ molecule can yield four molecules and one molecule of $H_2$ respectively, as indicated by reactions I, II and III in Eq.(10). We rewrite Eq.(16) with the following coordinate transformations,

$$U = 1 - \frac{\dot{N}_o\zeta_a}{\dot{N}_{in}\zeta_r}, \qquad \begin{aligned}\zeta_r &= 4\mathcal{X}_{1,r}+\mathcal{X}_{2,r}+\mathcal{X}_{4,r}\\ \zeta_a &= 4\mathcal{X}_{1,a}+\mathcal{X}_{2,a}+\mathcal{X}_{4,a}\end{aligned} \tag{17}$$

Using Eqs.(17), (8) and (14), $\zeta_r$ and $\zeta_a$ are expressed in the following state-space form:

$$\begin{gathered}
\dot{\mathbf{Z}} = \mathbf{A}_1\mathbf{Z}+\mathbf{B}_1,\ \mathbf{Z} = \left[\zeta_r, \zeta_a\right]^T,\\
\mathbf{A}_1 = \begin{bmatrix}-(\dot{N}_{in}+\dot{N}_r)/N_r & k\dot{N}_o/N_r\\ \dot{N}_{in}/N_a & -(\dot{N}_o+\dot{N}_a)/N_a\end{bmatrix},\\
\mathbf{B}_1 = \begin{bmatrix}4\dot{N}_f/N_r\\ -i\mathcal{N}_{cell}/nFN_a\end{bmatrix}
\end{gathered} \tag{18}$$

It is interesting to note here that Eq.(18) is devoid of the reaction rates $\mathcal{R}_{1,r}$, $\mathcal{R}_{2,r}$, $\mathcal{R}_{1,a}$, and $\mathcal{R}_{2,a}$. This is advantageous, but Eq.(18) is nonetheless nonlinear since $\dot{N}_{in}$, $\dot{N}_o$, $N_r$, $N_a$, $\dot{N}_r$, and $\dot{N}_a$ are nonlinear functions of mole fractions, temperatures and pressures as shown below

$$\begin{gathered}
\dot{N}_{in} = \dot{M}_{in}/\sum_{i=1}^{5}\mathcal{X}_{i,r}\,MW_i,\ \dot{N}_o = \dot{M}_o/\sum_{i=1}^{5}\mathcal{X}_{i,a}\,MW_i,\\
N_r = P_rV_r/R_uT_r,\ N_a = P_aV_a/R_uT_a
\end{gathered} \tag{19}$$

Since $\mathbf{Z}_{ss} = \mathbf{A}_1^{-1}\mathbf{B}_1$, from Eqs.(17) and (18) we obtain the following expression for steady-state utilization:

$$U_{ss} = \frac{1-k}{\left(4nF\dot{N}_f/i\mathcal{N}_{cell}\right)-k} \tag{20}$$

Note that Eq.(20) is independent of the variables in Eq.(19). Furthermore, since $k$, $i$ and $\dot{N}_f$ are measurable and known inputs, Eq.(20) can be used to exactly predict the steady-state fuel utilization for any given set of inputs.

## VI. A PRELIMINARY CONTROL STRATEGY

The steady-state relation in Eq.(20) can be utilized as a control law to achieve a target utilization $U_{ss}$. From Eq.(20) we have

$$\dot{N}_f = \frac{i\mathcal{N}_{cell}}{4nFU_{ss}}\left[1-\left(1-U_{ss}\right)k\right] \tag{21}$$

An advantage of the above control law is the minimal sensor requirement. However, this strategy is based on steady-state behavior. Hence we must assess its effectiveness in the presence of transient current demand. We consider a current surge in the form of a step change. For all simulations presented in this paper, we consider a 576 cell tubular SOFC system with 192 cells in series and three rows in parallel. The active area of each cell is $251\text{cm}^2$. Additional details and sample simulation data can be found in our earlier work [4], and references therein. The dynamics of fuel flow is considered unknown. However, to demonstrate its effect on transient, we choose a first order dynamics with a time constant of 2s and a ramped dynamics with a slope of $0.002$moles/s. In a fuel cell system, this effect typically results from the dynamics of a fuel pump, or mass flow controller, or valve [12]. The following simulation result shows the performance of the preliminary control implemented using Eq.(21). As shown

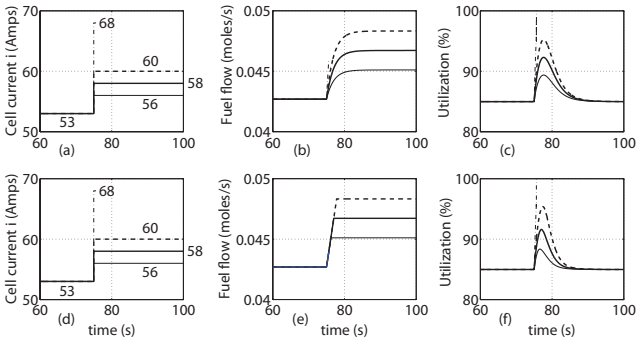


Fig. 4. Transient fuel utilization with preliminary control law

in Fig.4(a), multiple step changes in the current demand were applied. The corresponding changes in $\dot{N}_f$ are shown in Fig.4(b). Note the first order dynamics in $\dot{N}_f$ in Fig.4(b). The target steady-state utilization $U$ was set at $85\%$. Fig.4(c) shows significant deviation of $U$ from its target following the current surge. Note that both the magnitude and the duration of deviation are considerable and is accentuated with increase in the step. This behavior is not exclusive to a first order dynamics but a common observation for any type of dynamics applied to emulate the fuel flow, such as the ramped dynamics shown in Figs.4(d), (e) and (f). The transient $U$ shown above is detrimental. In applications where fast power transients are frequent, such transients in $U$ can cause rapid degradation of fuel cell stack through drop in cell voltage and anode oxidation. In the next section, we develop a feedback based current shaping strategy that will mitigate the issue illustrated above.

## VII. FEEDBACK BASED LOAD SHAPING STRATEGY

To alleviate the issue of excessive transients in the fuel utilization, our proposed strategy uses feedback to dynamically shape the current draw from the fuel cell system. Denoting the net current demand as $i_{fc,d}$, the corresponding fuel demand $\dot{N}_{f,d}$ is derived from Eq.(21) as follows:

$$\dot{N}_{f,d} = \frac{i_{fc,d}\mathcal{N}_{cell}}{4nFU_{ss}}\left[1-(1-U_{ss})\,k\right] \tag{22}$$

The actual fuel flow, denoted by $\dot{N}_{f,m}$, is dependent on actuator dynamics and hence, at least during the transient, is different from $\dot{N}_{f,d}$. The fuel cell current draw, $i_{fc}$, is now determined based on $\dot{N}_{f,m}$ as follows

$$i_{fc} = \frac{4nFU_{ss}\dot{N}_{f,m}}{\mathcal{N}_{cell}}\,\frac{1}{[1-(1-U_{ss})\,k]} \tag{23}$$

This current draw is achieved using current control in the associated power electronics of the fuel cell system. The response of power electronics components such as DC/DC converters are typically much faster compared to that of the fuel cell and hence their dynamics are neglected in the control design. The overall control scheme is depicted in Fig.5. The approach requires just one additional sensor, namely a flowrate sensor that measures $\dot{N}_f$, which is typically available in fuel cells.

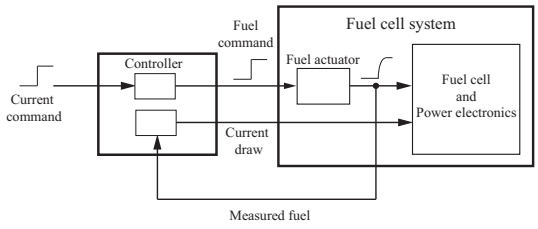


Fig. 5. Scheme for transient utilization control

In Fig.6, we demonstrate the performance of the proposed control strategy for the same step changes in current demand as shown in Fig.4. The fuel cell current $i_{fc}$ follows $\dot{N}_{f,m}$, as

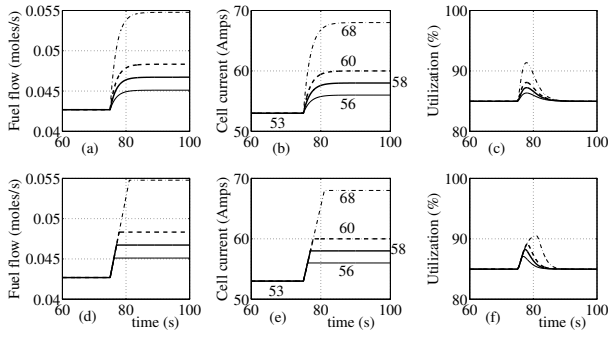


Fig. 6. Transient fuel utilization with load shaping strategy

shown in Figs.6(a) and (b), and in Figs.6(d) and (e), instead of undergoing a step change. This dynamic shaping of $i_{fc}$ significantly reduces the transients in $U$, shown in Figs.6(c) and (f). To establish the effectiveness of this control strategy, we have applied it across a variety of fuel flow dynamics and current demand profiles. Note that the dynamic shaping based on the measurement of $\dot{N}_f$ only and does not require a prior knowledge of fuel flow dynamics.

## VIII. A SAMPLE HYBRID FUEL CELL SYSTEM

It is evident from the discussion above that during transients, $i_{fc}$ will be dynamically shaped to reduce fluctuations in $U$ from the target value. This will lead to a mismatch between the demanded power and fuel cell delivered power. This is a fitting scenario to consider a hybrid fuel cell system with a supplementary power source such as a battery or a super-capacitor. Thus during transient operation, while the proposed control strategy will ensure that the fuel utilization undergoes minimal deviation from $U_{ss}$, the power deficit or surplus will be managed by discharging or charging the supplementary power source. In this section, we extend our proposed algorithm to consider power split in a hybrid fuel cell system. A schematic diagram of a hybrid fuel cell system is shown in Fig.7.

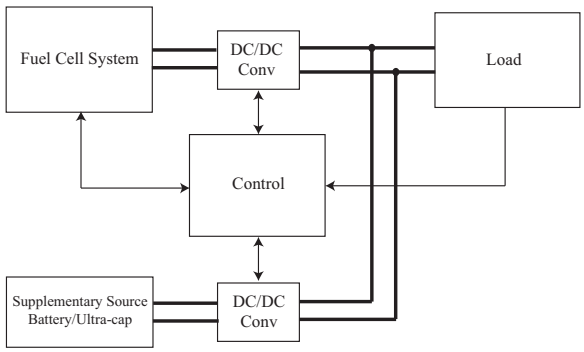


Fig. 7. Hybrid fuel cell system

In addition to controlling the transient utilization, the power split control algorithm must also maintain the State-Of-Charge (SOC) of the battery or super-capacitor. The later aspect of the control law is under development and hence not presented in this paper. Let us consider a net power demand of $P_{net}$. Since this power demand is met by the combined system, we have

$$P_{net} = \eta_{fc}V_{fc}i_{fc} + \eta_s V_s i_s \tag{24}$$

where $\eta_{fc}$ and $\eta_s$ are the efficiencies of the DC/DC converters dedicated to the fuel cell and supplementary source respectively. Also, $V_s$ and $i_s$ are the voltage and current draw of the supplementary power source. Since $i_{fc}$ must follow the actual fuel flow $\dot{N}_{f,m}$, from Eqs.(23) and (24) the required supplementary current draw $i_s$ is given by

$$i_s = \left[P_{net} - \eta_{fc}V_{fc}\frac{4nFU_{ss}\dot{N}_{f,m}}{\mathcal{N}_{cell}}\,\frac{1}{1-(1-U_{ss})\,k}\right]/\eta_s V_s \tag{25}$$

The above equation incorporates our feedback based input shaping control strategy. The fuel cell current demand $i_{fc,d}$ is based on $P_{net}$, as follows:

$$i_{fc,d} = P_{net}/\eta_{fc}V_{fc} \tag{26}$$

This equation will be modified as we address the control of battery/super-capacitor SOC which is an area of ongoing research. From Eqs.(22) and (26), the demanded fuel flow in the fuel cell is given by

$$\dot{N}_{f,d} = \frac{P_{net}\mathcal{N}_{cell}}{4nFU_{ss}\eta_{fc}V_{fc}}\left[1-(1-U_{ss})\,k\right] \qquad (27)$$

The preliminary control strategy for the hybrid system outlined above is tested in a simulation. In the simulation we have modeled a Li-ion battery as the supplementary power source with the connectivity shown in Fig.7. The simulation results are shown in Fig.8. In this simulation, a step increase

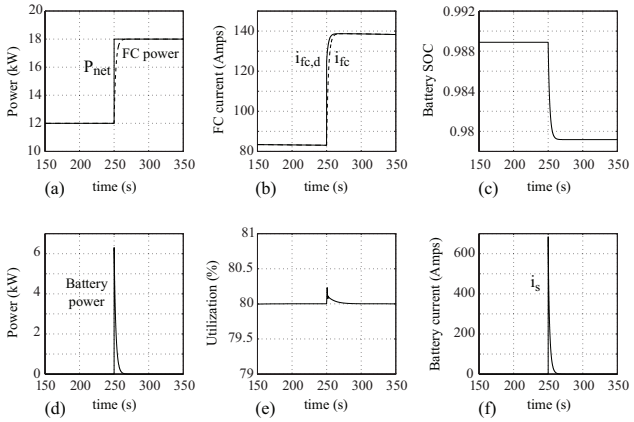


Fig. 8. Performance of power-split strategy

was applied to the net power demand, from 12kW to 18kW, as shown in Fig.8(a). The resulting demanded and actual fuel cell currents are shown in Fig.8(b). The actual fuel cell current draw lags the target current since it follows the measured fuel flow. As a result of this, the power delivered by the fuel cell is lower than the power demand as shown in Fig.8(a) during the transient phase. The dynamic current shaping causes minor deviation of $U$ from the target value of $80\%$, Fig.8(e). The power deficit during transient phase is delivered by the battery, Fig.8(d). The corresponding battery current and change in SOC are given in Figs.8(f) and (c) respectively.

## IX. CONCLUSIONS

In this paper we present a control strategy for reducing fluctuations in fuel utilization in Solid Oxide Fuel Cell systems arising from drastic load transients. Fuel utilization is a non-linear function of concentrations of several gaseous species in the SOFC system and hence require several sensors for accurate measurement and control. In our approach, we address fuel utilization control using closed-form relations derived from a model-based analysis. These relations are then combined with sensor measurements to form a feedback based dynamic load-shaping strategy. The sensing required for implementing this strategy is the measurement of fuel flow $\dot{N}_f$, which is typically available in fuel cell systems. The control design is shown to significantly reduce transients in utilization, thereby establishing tight control around a target value. The strategy fits directly into the design of a comprehensive power split control algorithm for a hybrid SOFC and battery/super-capacitor system. This is an area of ongoing and future research.

## X. ACKNOWLEDGMENTS

The authors gratefully acknowledge the support provided by the Office of Naval Research, grant #N000140810704, in conducting this research.

## REFERENCES

[1] http://www.epa.gov/otaq/emisslab/testing/dynamometer.htm.

[2] M. Y. Ayad, M. Becharif, A. Djerdir, and A. Miraoui. Sliding mode control for energy management of dc hybrid power sources using fuel cell, batteries and supercapacitors. *International Conference on Clean Electrical Power*, pages 500–505, 2007.

[3] R. Bove, P Lunghi, and N. M. Sammes. SOFC mathematic model for systems simulations - part 2: Definition of an analytical model. *International Journal of Hydrogen Energy*, 30:189–200, 2005.

[4] T. Das, S. Narayanan, and R. Mukherjee. Model based characterization of transient response of a solid oxide fuel cell system. *ASME International Mechanical Engineering Congress and Exposition*, pages 655–664, 2007.

[5] A. Drolia, P. Jose, and N. Mohan. An approach to connect ultracapacitor to fuel cell powered electric vehicle and emulating fuel cell electrical characteristics using switched mode converter. *Proceedings of Industrial Electronics Conference*, pages 897–901, 2003.

[6] M. L. Ferrari, A. Traverso, L. Magistri, and A. F. Massardo. Influence of anodic recirculation transient behavior on the SOFC hybrid system performance. *Journal of Power Sources*, 149:22–32, 2005.

[7] A. Hajizadeh and M. A. Golkar. Intelligent power management strategy of hybrid distributed generation systems. *Electrical Power and Energy Systems*, 29:783–795, 2007.

[8] F. P. Incropera and D. P. DeWitt. *Fundamentals of Heat and Mass Transfer*. John Wiley & Sons, Inc., fifth edition, 2002.

[9] Z. Jiang, L. Gao, and R. A. Dougal. Adaptive control strategy for active power sharing in hybrid fuel cell/battery power sources. *IEEE Transactions on Energy Conversion*, 22(2):507–515, 2007.

[10] R. Kandepu, L. Imsland, B. A. Foss, C. Stiller, B. Thorud, and O. Bolland. Modeling and control of a SOFC-GT-based autonomous power system. *Energy*, 32:406–417, 2007.

[11] J. R. Meacham, F. Jabbari, J. Brouwer, J. L. Mauzey, and G. Scott Samuelsen. Analysis of stationary fuel cell dynamic ramping capabilities and ultra capacitor energy storage using high resolution demand data. *Journal of Power Sources*, 156:472–479, 2006.

[12] F. Mueller, J. Brouwer, F. Jabbari, and S. Samuelsen. Dynamic simulation of an integrated solid oxide fuel cell system including current-based fuel flow control. *ASME Journal of Fuel Cell Science and Technology*, 3:144–154, 2006.

[13] S. Narayanan. Steady-state and transient analysis of a steam reformer based solid oxide fuel cell system. *MS Thesis, Michigan State University*, 2008.

[14] V. Paladini, T. Donateo, A. de Risi, and D. Laforgia. Super-capacitor fuel-cell hybrid electric vehicle optimization and control strategy development. *Energy Conversion and Management*, 48:3001–3008, 2007.

[15] P. Thounthong, S. Rael, and B. Davat. Control strategy of fuel cell/supercapacitors hybrid power sources for electric vehicle. *Journal of Power Sources*, 158:806–814, 2006.

[16] M. Uzunoglu and M. S. Alam. Dynamic modeling, design and simulation of a pem fuel cell/ultracapacitor hybrid system for vehicular applications. *Energy Conversion and Management*, 48:1544–1553, 2007.

[17] A. Vahidi, I Kolmanovsky, and A Stefanopoulou. Constraint handling in fuel cell system: A fast reference governor approach. *IEEE Transactions on Control Systems Technology*, 15(1):86–98, 2007.

[18] J. Xu and G. F. Froment. Methane steam reforming, methanation and water-gas shift: I. Intrinsic kinetics. *AIChE Journal*, 35(1):88–96, 1989.